



HAL
open science

Multi-material topology optimization of structural load-bearing capacity using limit analysis

Leyla Mourad, Jeremy Bleyer, Romain Mesnil, Joanna Nseir, Karam Sab, Wassim Raphael

► To cite this version:

Leyla Mourad, Jeremy Bleyer, Romain Mesnil, Joanna Nseir, Karam Sab, et al.. Multi-material topology optimization of structural load-bearing capacity using limit analysis. 2022. hal-03528107v1

HAL Id: hal-03528107

<https://enpc.hal.science/hal-03528107v1>

Preprint submitted on 17 Jan 2022 (v1), last revised 5 Feb 2024 (v3)

HAL is a multi-disciplinary open access archive for the deposit and dissemination of scientific research documents, whether they are published or not. The documents may come from teaching and research institutions in France or abroad, or from public or private research centers.

L'archive ouverte pluridisciplinaire **HAL**, est destinée au dépôt et à la diffusion de documents scientifiques de niveau recherche, publiés ou non, émanant des établissements d'enseignement et de recherche français ou étrangers, des laboratoires publics ou privés.

Multi-material topology optimization of structural load-bearing capacity using limit analysis

Leyla Mourad · Jeremy Bleyer · Romain Mesnil · Joanna Nseir ·
Karam Sab · Wassim Raphael

Received: date / Accepted: date

Abstract We extend the problem of finding an optimal structure with maximum load-bearing capacity to the case of multiple materials. We first consider a reinforcement optimization case where the structure consists of a fixed background matrix material with given strength properties and optimize the reinforcement topology within this material. We discuss the use of various isotropic and anisotropic strength criteria to model the reinforcing phase, including reinforcements with discrete orientations. In a second time, we investigate a bi-material formulation where we optimize the topology of two material phases simultaneously. Various choices for the material strength conditions are proposed and we apply this formulation to the optimization of pure tensile and compressive phases of a single material. In all cases, two optimization variants are proposed using concepts of convex optimization and limit analysis theory, namely maximizing the load-bearing capacity under a fixed volume constraint or minimizing the volume under a fixed loading. Both problems are convex and a penalization procedure is proposed. The underlying problems can be solved using conic programming solvers. Illustrative applications demonstrate the versatility of the proposed formulation, including the influence of the selected strength criteria, the possibility to

obtain structures with members of fixed orientation or structures with different importance granted to tensile and compressive regions. Finally, we also draw a parallel with the generation of strut-and-tie models for the analysis of reinforced concrete structures.

Keywords Topology optimization · Limit Analysis · Homogenization · Bearing capacity · Second-order cone programming · No-tension material

Funding Information

This work is part of the PhD thesis of L. Mourad who is supported by Université Paris-Est and Université Saint-Joseph.

1 Introduction

Although topology optimization methods have become increasingly popular, many works concentrate on compliance optimization of elastic materials. Plastic design optimization has been much less investigated although fundamental theoretical works have dealt with both elastic and plastic design [35, 39, 43]. Despite nonlinear constitutive relations having been considered in the topology optimization process [3, 4, 27, 44, 48], the numerical cost is very high and there are still many difficulties to be tackled when including local stress constraints [15, 33]. In contrast, plastic design of truss structures [14, 19, 21] shows less problems and is now able to tackle large scale problems with the development of efficient linear programming solvers. Interestingly, the extension of the concepts of plastic truss design to continuum topology optimization has been largely ignored until recently when strength-based

L. Mourad · J. Bleyer (✉) · R. Mesnil · K. Sab
Laboratoire Navier, Ecole des Ponts ParisTech, Univ Gustave Eiffel, CNRS
6-8 av. Blaise Pascal, Cité Descartes
77455 Champs-sur-Marne, France
Tel : +33 (0)1 64 15 37 43
E-mail: jeremy.bleyer@enpc.fr

L. Mourad · J. Nseir · W. Raphael
Université Saint Joseph, Faculté des sciences, Mar Roukos-Dekwaneh, Lebanon

topology optimization of von Mises plastic materials were proposed [16, 22, 23]. In a more general manner using the concepts of limit analysis, we formulated in [30] the problem of maximizing a structure’s load-bearing capacity subject to given material strength properties and a material volume constraint. This problem is also closely linked to the problem of minimizing the total volume under the constraint of carrying a fixed loading as well as to Michell’s theory of optimal trusses [28]. In particular, this approach, which relies on convex optimization solvers, enables to treat the case of materials with different strength properties in tension and compression which are commonly encountered in civil engineering applications.

Apart from topology optimization, interesting mechanical performances can be achieved when mixing materials with different mechanical properties, motivating the extension of topology optimization approaches towards the multi-material case. For instance, the density-based SIMP methodology was extended to multiple material phases in various works [18, 20, 41, 53] whereas others used a phase-field approach based on Allen-Cahn or Cahn-Hilliard models [45, 47, 52] or level-set methods [1, 24]. Only few works considered multi-material topology optimization with material non-linearity such as [38, 49, 50]. The extension of continuous plastic-based (or limit-analysis based) topology optimization to multi-materials, which is the main purpose of the present work, has never been done.

As it will be illustrated later, our work also bears conceptual similarities with the so-called *strut-and-tie method* frequently used for the ultimate design of reinforced concrete (RC) structures using a truss analogy [32, 37, 40]. Compressed concrete regions are idealized as compressive struts and steel rebars as tensile ties, both of them experiencing uniaxial stress states and connecting to each other at nodes which sustain multi-axial stress states. The Strut-and-Tie (ST) method is used in common engineering practice as a hand-based procedure to verify a RC structure bearing capacity once the ST model has been established. It is also used, at an earlier stage of the design, to find an efficient layout of steel rebars by considering different ST models. Optimizing for the steel rebars position is difficult to automate since it also strongly depends on the compressive struts’ layout. Previous works proposed to identify a ST model based on the flow of elastic stresses of the continuous structure [12, 26] or by optimizing for the structure compliance using topology optimization concepts [8, 17], arguing

that a stiff structure exhibits the best load-deformation behavior. Only few references such as [9, 36, 42, 46] generated ST models using topology optimization by considering different tensile and compressive properties for steel and concrete phases. We can also mention references based on a ground-structure layout optimization approach [11, 42, 51]. Overall, the majority of such works are based on compliance minimization.

Our contribution therefore aims at bridging the gap between multi-material topology optimization, plastic or limit analysis-based topology optimization and the generation of strut-and-tie like models using materials with different tensile and compressive strengths. Doing so, we aim at formulating a generic framework for the optimization of the load-bearing capacity of reinforced structures, either by considering a fixed background matrix material and optimizing for the reinforcing phase only or by simultaneously optimizing for the topology of two different phases (in addition to a potential void phase). As it will be seen, this second possibility will offer a natural framework for the generation of strut-and-tie models by considering tensile-only and compression-only phases. Following the same spirit as our previous work [30], our approach will be strongly based on the concepts of convex optimization, especially regarding the formulation of isotropic and anisotropic strength conditions promoting specific features such as uniaxial or pure tension/compression stress states. As a result, our numerical implementation uses convex optimization solvers and solves simultaneously for the mechanical state and the optimal density field(s), thereby avoiding the need to compute sensitivities for instance.

The present manuscript is organized as follows: section 2 first recalls concepts and notations of the limit analysis-based topology optimization methodology proposed in [30], section 3 then discusses its extension to reinforcement optimization and the choice of a strength condition for the reinforcement phase, section 4 presents a bimaterial formulation optimizing two material phases in addition to a void phase and similarly discusses different possible choices of strength criteria for both phases and section 5 finally discusses the numerical aspects and presents various illustrative applications of the proposed approach.

2 A review of limit analysis-based topology optimization

In this section, we recall the general concepts of limit analysis-based topology optimization introduced

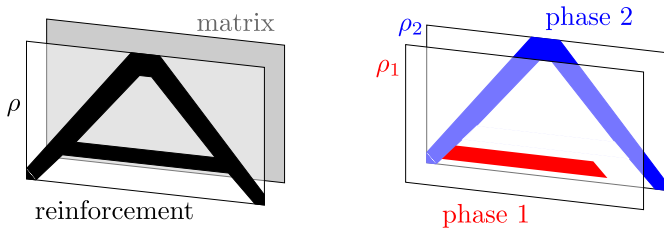


Fig. 1: Two variants of multi-material optimization. Left: reinforcement optimization where the background "matrix" material is fixed and we optimize a single "reinforcement" phase, right: general bi-material optimization where we optimize over two materials and a void phase

in [30], see also [16, 22, 23] for similar formulations.

First, limit analysis aims at finding the maximum load amplification factor λ for which there exists an internal stress field $\boldsymbol{\sigma}$ which can balance the loading and still comply with the material strength criterion $\boldsymbol{\sigma} \in G$ at every point in the domain Ω . Here, G is a convex set containing 0 which represents the material strength properties e.g. a plastic yield criterion. According to such a characterization, the limit load Λ^+ can be found as the solution to the following convex optimization problem:

$$\begin{aligned} \Lambda^+ = \max_{\lambda, \boldsymbol{\sigma}} \lambda \\ \text{s.t. } \operatorname{div} \boldsymbol{\sigma} = 0 \quad \text{in } \Omega \\ \boldsymbol{\sigma} \cdot \mathbf{n} = \lambda \mathbf{T} \quad \text{on } \partial\Omega_T \\ \boldsymbol{\sigma} \in G \quad \text{in } \Omega \end{aligned} \quad (1)$$

in which we neglect body forces for simplicity and look for the maximal value of the reference surface tractions \mathbf{T} acting on some part $\partial\Omega_T$ of the boundary.

2.1 A load-maximization problem

Considering a computational domain \mathcal{D} , we proposed in [30] an extension of the concepts of limit analysis to the determination of an optimized structure $\Omega \subseteq \mathcal{D}$ which would have the maximum load-bearing capacity for a given material volume fraction constraint $|\Omega| \leq \eta|\mathcal{D}|$. Formulating this problem as a non-convex binary optimization problem and considering its convexification through a continuous pseudo-

density $\rho(\mathbf{x}) \in [0; 1]$, we define the following load-maximization problem:

$$\begin{aligned} \lambda^+ = \max_{\lambda, \boldsymbol{\sigma}, \rho} \lambda \\ \text{s.t. } \operatorname{div} \boldsymbol{\sigma} = 0 \quad \text{in } \mathcal{D} \\ \boldsymbol{\sigma} \cdot \mathbf{n} = \lambda \mathbf{T} \quad \text{on } \partial\mathcal{D}_T \\ \boldsymbol{\sigma} \in \rho G \quad \text{in } \mathcal{D} \\ \int_{\mathcal{D}} \rho \, dx \leq \eta|\mathcal{D}| \\ 0 \leq \rho \leq 1 \end{aligned} \quad (\text{LOAD-MAX})$$

where the main difference with (1) comes from the density-dependent strength criterion ρG . Clearly, when $\rho = 0$, we have $\boldsymbol{\sigma} = 0$ and when $\rho = 1$, $\boldsymbol{\sigma} \in G$ which correspond to the initial material strength condition. Finally, one key property of the above problem is that it is convex and can be solved using dedicated conic programming solvers for many usual strength criteria.

2.2 A related volume-minimization problem

Finally, for a fixed loading level λ , one can also find the structure sustaining the loading with the minimum volume. A similar volume-minimization problem therefore reads as [22, 23]:

$$\begin{aligned} \eta^- = \min_{\boldsymbol{\sigma}, \rho} \frac{1}{|\mathcal{D}|} \int_{\mathcal{D}} \rho \, dx \\ \text{s.t. } \operatorname{div} \boldsymbol{\sigma} = 0 \quad \text{in } \mathcal{D} \\ \boldsymbol{\sigma} \cdot \mathbf{n} = \lambda \mathbf{T} \quad \text{on } \partial\mathcal{D}_T \\ \boldsymbol{\sigma} \in \rho G \quad \text{in } \mathcal{D} \\ 0 \leq \rho \leq 1 \end{aligned} \quad (\text{VOL-MIN})$$

which is again a convex problem.

2.3 Choice of the material strength criterion

The choice of the material strength criterion G will have an important impact on the optimal design. For instance, criteria with anisotropic strength properties will induce anisotropic features in the optimized design. Regarding isotropic materials, the optimized structure load-capacity depends essentially upon the material uniaxial tensile (resp. compressive) strength f_t (resp. f_c). Indeed, optimized topologies usually have a truss-like layout with many members subjected to uniaxial stress states. In [30], the so-called L_1 -Rankine criterion was introduced as follows:

$$\boldsymbol{\sigma} \in G^{L_1\text{-Rankine}} \Leftrightarrow g(\sigma_I) + g(\sigma_{II}) \leq 1 \quad (2)$$

written here in 2D with σ_I , σ_{II} being the principal stresses and where:

$$g(\sigma) = \max \left\{ -\frac{\sigma}{f_c}; \frac{\sigma}{f_t} \right\} \quad (3)$$

It was advocated in [30] that the L_1 -Rankine criterion was a good choice for promoting uniaxial stress states in the optimal solutions. This argument will be revisited in section 3.4.

3 Reinforcement material optimization

In this section, we investigate the situation in which we optimize a single phase with a fixed background phase (see Figure 1-left). This situation essentially applied to the optimization of a reinforcing phase in a composite material, the background fixed phase then corresponding to the matrix material. We will respectively denote by G^m and G^r the strength criteria of the matrix and reinforcement bulk materials.

3.1 Reinforced material strength conditions

In general, reinforcements are present in a small volume fraction $\phi \ll 1$. In such a case, the strength criterion of the composite material G^{comp} can be approximated by the following dilute estimation:

$$G^{\text{comp}} = (1 - \phi)G^m \oplus \phi G^r \quad (4)$$

where \oplus denotes the Minkowski sum between two sets¹. As a result, the stress field $\boldsymbol{\sigma}$ can be decomposed as the sum of a matrix and a reinforcement partial stress as follows:

$$\boldsymbol{\sigma} \in G^{\text{comp}} \Leftrightarrow \exists \boldsymbol{\sigma}^m, \boldsymbol{\sigma}^r \text{ s.t. } \begin{cases} \boldsymbol{\sigma} = \boldsymbol{\sigma}^m + \boldsymbol{\sigma}^r \\ \boldsymbol{\sigma}^m \in (1 - \phi)G^m \\ \boldsymbol{\sigma}^r \in \phi G^r \end{cases} \quad (5)$$

Accounting for the fact that $\phi \ll 1$, the above expression can even be further simplified as follows:

$$\boldsymbol{\sigma} \in G^{\text{comp}} \Leftrightarrow \exists \boldsymbol{\sigma}^m, \boldsymbol{\sigma}^r \text{ s.t. } \begin{cases} \boldsymbol{\sigma} = \boldsymbol{\sigma}^m + \boldsymbol{\sigma}^r \\ \boldsymbol{\sigma}^m \in G^m \\ \boldsymbol{\sigma}^r \in G^{r,\text{eff}} \end{cases} \quad (6)$$

where $G^{r,\text{eff}} = \phi G^r$. This formulation states that the composite strength condition corresponds to a stress state which is the sum of a stress $\boldsymbol{\sigma}^m$ satisfying the bulk matrix condition and a contribution of the effective strength condition of the reinforcement material, the strength property of which being that of the bulk reinforcement material scaled by the reinforcement volume fraction.

Although the following approach of section 3.2 can be easily considered for a strength criterion of the form (5), we will now only consider the simplified form (6).

3.2 Convex problems formulation

We assume here that the matrix material is fixed and occupies the whole computational domain \mathcal{D} and we aim at optimizing over the reinforcement phase only. The approach of [30] can be easily extended by considering the following density-dependent composite strength criterion:

$$\begin{aligned} \boldsymbol{\sigma} \in G^{\text{comp}}(\rho) &= G^m \oplus \rho G^{r,\text{eff}} \\ \Leftrightarrow \exists \boldsymbol{\sigma}^m, \boldsymbol{\sigma}^r \text{ s.t. } &\begin{cases} \boldsymbol{\sigma} = \boldsymbol{\sigma}^m + \boldsymbol{\sigma}^r \\ \boldsymbol{\sigma}^m \in G^m \\ \boldsymbol{\sigma}^r \in \rho G^{r,\text{eff}} \end{cases} \end{aligned} \quad (7)$$

such that we still have $G^{\text{comp}}(\rho = 1) = G^{\text{comp}}$. The main difference with the single material optimization for which $G(0) = \{0\}$ was representing void is that we now have $G^{\text{comp}}(\rho = 0) = G^m$. As a result, the above strength criterion will interpolate for $\rho \in [0; 1]$ between the pure matrix strength condition G^m and the reinforced composite criterion G^{comp} .

The two corresponding load-maximization (LOAD-MAX) and volume minimization (VOL-MIN) problems are therefore respectively given by:

$$\begin{aligned} \lambda^+ &= \max_{\lambda, \boldsymbol{\sigma}^m, \boldsymbol{\sigma}^r, \rho} \lambda \\ \text{s.t. } &\begin{cases} \text{div}(\boldsymbol{\sigma}^m + \boldsymbol{\sigma}^r) = 0 & \text{in } \mathcal{D} \\ (\boldsymbol{\sigma}^m + \boldsymbol{\sigma}^r) \cdot \mathbf{n} = \lambda \mathbf{T} & \text{on } \partial \mathcal{D}_T \\ \boldsymbol{\sigma}^m \in G^m & \text{in } \mathcal{D} \\ \boldsymbol{\sigma}^r \in \rho G^{r,\text{eff}} & \text{in } \mathcal{D} \\ \int_{\mathcal{D}} \rho \, dx \leq \eta |\mathcal{D}| \\ 0 \leq \rho \leq 1 \end{cases} \end{aligned} \quad (\text{REINF-LOAD-MAX})$$

and

$$\begin{aligned} \eta^- &= \min_{\boldsymbol{\sigma}^m, \boldsymbol{\sigma}^r, \rho} \frac{1}{|\mathcal{D}|} \int_{\mathcal{D}} \rho \, dx \\ \text{s.t. } &\begin{cases} \text{div}(\boldsymbol{\sigma}^m + \boldsymbol{\sigma}^r) = 0 & \text{in } \mathcal{D} \\ (\boldsymbol{\sigma}^m + \boldsymbol{\sigma}^r) \cdot \mathbf{n} = \lambda \mathbf{T} & \text{on } \partial \mathcal{D}_T \\ \boldsymbol{\sigma}^m \in G^m & \text{in } \mathcal{D} \\ \boldsymbol{\sigma}^r \in \rho G^{r,\text{eff}} & \text{in } \mathcal{D} \\ 0 \leq \rho \leq 1 \end{cases} \end{aligned} \quad (\text{REINF-VOL-MIN})$$

where the total stress $\boldsymbol{\sigma}$ has been replaced by the sum of the two partial stresses arising in the definition (7). As a result, both problems are very similar to the single material counterpart, which can be obtained in the particular case $\boldsymbol{\sigma}^m = 0$. The numerical implementation, including the penalty procedure, will therefore be a straightforward adaptation to that described in [30]. Note in particular that only a global

¹ $A \oplus B = \{a + b \text{ s.t. } a \in A, b \in B\}$

equilibrium condition on the total stress $\boldsymbol{\sigma} = \boldsymbol{\sigma}^m + \boldsymbol{\sigma}^r$ needs to be considered so that standard finite-element discretization can be used to enforce this equation weakly.

Before finishing this section, let us now discuss some particular choices for $G^{r,\text{eff}}$ in the case of uniaxial reinforcements.

3.3 The particular case of uniaxial reinforcements

The dilute estimation (5) always provides an upper bound to the real homogenized strength condition of the composite material. When considering uniaxial reinforcements aligned along a direction \mathbf{e}_α , this upper bound can be improved. In the case of small volume fraction, the composite homogenized strength criterion is in fact exactly given by [10, 13]:

$$\boldsymbol{\sigma} \in G^{\text{comp}} \Leftrightarrow \exists \boldsymbol{\sigma}^m, \sigma^r \text{ s.t. } \begin{cases} \boldsymbol{\sigma} = \boldsymbol{\sigma}^m + \sigma^r \mathbf{e}_\alpha \otimes \mathbf{e}_\alpha \\ \boldsymbol{\sigma}^m \in G^m \\ -f_c^{r,\text{eff}} \leq \sigma^r \leq f_t^{r,\text{eff}} \end{cases} \quad (8)$$

where $f_t^{r,\text{eff}}$ (resp. $f_c^{r,\text{eff}}$) denotes the reinforcement uniaxial effective tensile (resp. compressive) strength (per unit of transverse area). As a result, the case of uniaxial reinforcements is similar to (6) except that the effective reinforcement strength criterion $G^{r,\text{eff}}$ is now given by the corresponding uniaxial strength condition:

$$G^{r,\text{eff}} = \{\sigma^r \mathbf{e}_\alpha \otimes \mathbf{e}_\alpha \text{ s.t. } -f_c^{r,\text{eff}} \leq \sigma^r \leq f_t^{r,\text{eff}}\} \quad (9)$$

Finally, the homogenized strength criterion (8) and (9) easily generalize to a reinforcing material made of multiple reinforcement directions by summing the corresponding uniaxial stress contributions. For instance, an important practical case of interest is that of orthogonal reinforcements aligned with the global x, y directions (and possibly z in 3D). In this case, the effective strength criterion (9) for two reinforcement directions \mathbf{e}_x and \mathbf{e}_y generalizes to:

$$G^{r,\text{eff}} = \{\sigma^{r,x} \mathbf{e}_x \otimes \mathbf{e}_x + \sigma^{r,y} \mathbf{e}_y \otimes \mathbf{e}_y \text{ s.t. } -f_c^{r,\text{eff}} \leq \sigma^{r,x}, \sigma^{r,y} \leq f_t^{r,\text{eff}}\} \quad (10)$$

3.4 The L_1 -Rankine criterion for isotropically distributed reinforcements

Similarly to the concepts of the homogenization method in topology optimization, our ultimate goal is to find an optimal microstructure for the reinforcing

phase at each material point. To do so, instead of considering that the reinforcing material is made of a fixed distribution of predefined orientations, we can consider a reinforcing material consisting of uniaxial reinforcements but with locally unknown orientation *a priori*, with the goal that the topology optimization process would naturally select the locally optimal orientation. In [30], the use of a L_1 -Rankine was proposed in order to promote uniaxial stress fields. Let us now revisit this argument and exhibit the link with a material made of isotropically distributed uniaxial reinforcements.

Let us indeed consider that the reinforcing material is made of a distribution of uniaxial reinforcements belonging to a certain family \mathcal{A} of orientations α and of similar effective tensile/compressive strengths $f_t^{r,\text{eff}}, f_c^{r,\text{eff}}$. In order to enforce that only one orientation is active at a given material point, we can write the following strength condition:

$$\exists \sigma^{r,\alpha}, \zeta_\alpha \text{ s.t. } \begin{cases} \boldsymbol{\sigma}^r = \sum_{\alpha \in \mathcal{A}} \zeta_\alpha \sigma^{r,\alpha} \mathbf{e}_\alpha \otimes \mathbf{e}_\alpha \\ -f_c^{r,\text{eff}} \leq \sigma^{r,\alpha} \leq f_t^{r,\text{eff}} & \forall \alpha \in \mathcal{A} \\ \zeta_\alpha \in \{0; 1\} & \forall \alpha \in \mathcal{A} \\ \sum_{\alpha \in \mathcal{A}} \zeta_\alpha = 1 \end{cases} \quad (11)$$

where we introduced the binary variables ζ_α which describe the activation or not of a specific orientation, the last constraint enforcing that only one such orientation can be active.

Clearly, criterion (11) is non-convex due to the binary constraint on the ζ_α variable which will result in the corresponding topology optimization problem being extremely difficult to solve. To alleviate this issue and follow the same kind of convex optimization methodology of our approach, a natural idea is to convexify $G^{r,\text{eff}}$ by relaxing the binary constraint. We therefore consider the following convexified formulation:

$$\boldsymbol{\sigma}^r \in G^{r,\text{eff}} \Leftrightarrow \exists \sigma^{r,\alpha}, \zeta_\alpha \text{ s.t. } \begin{cases} \boldsymbol{\sigma}^r = \sum_{\alpha \in \mathcal{A}} \zeta_\alpha \sigma^{r,\alpha} \mathbf{e}_\alpha \otimes \mathbf{e}_\alpha \\ -f_c^{r,\text{eff}} \leq \sigma^{r,\alpha} \leq f_t^{r,\text{eff}} & \forall \alpha \in \mathcal{A} \\ 0 \leq \zeta_\alpha \leq 1 & \forall \alpha \in \mathcal{A} \\ \sum_{\alpha \in \mathcal{A}} \zeta_\alpha = 1 \end{cases} \quad (12)$$

which we recognize as the definition of the *convex hull* of the individual uniaxial strength conditions $G^\alpha = \{\sigma^{r,\alpha} \mathbf{e}_\alpha \otimes \mathbf{e}_\alpha \text{ s.t. } -f_c^{r,\text{eff}} \leq \sigma^{r,\alpha} \leq f_t^{r,\text{eff}}\}$ i.e.

$$G^{r,\text{eff}} = \text{conv}_{\alpha \in \mathcal{A}} \{G^\alpha\} \quad (13)$$

which is indeed the tightest convexification of the union of all the G^α . Finally, in the case where \mathcal{A} spans all the possible directions in space, we can easily show that $G^{\text{r,eff}}$ is in fact equal to the L_1 -Rankine criterion with tensile (resp. compressive) strength $f_t^{\text{r,eff}}$ (resp. $f_c^{\text{r,eff}}$) introduced in [30], see Appendix A for the proof. This result justifies that the L_1 -Rankine is the tightest convex criterion promoting uniaxial stress states in an isotropic fashion.

In the case of orthogonal reinforcements where α can only be aligned with either the x or y directions, the above convexified formulation (12) reads:

$$\begin{aligned} \boldsymbol{\sigma}^{\text{r}} \in G^{\text{r,eff}} &\Leftrightarrow \exists \sigma^{\text{r},x}, \sigma^{\text{r},y}, \zeta_x, \zeta_y \\ \text{s.t.} \quad &\begin{cases} \boldsymbol{\sigma}^{\text{r}} = \zeta_x \sigma^{\text{r},x} \mathbf{e}_x \otimes \mathbf{e}_x + \zeta_y \sigma^{\text{r},y} \mathbf{e}_y \otimes \mathbf{e}_y \\ -f_c^{\text{r,eff}} \leq \sigma^{\text{r},x}, \sigma^{\text{r},y} \leq f_t^{\text{r,eff}} \\ 0 \leq \zeta_x, \zeta_y \leq 1 \\ \zeta_x + \zeta_y = 1 \end{cases} \end{aligned} \quad (14)$$

Interestingly, the above criterion corresponds exactly to the L_1 -Rankine criterion intersected with the plane $\sigma_{xy}^{\text{r}} = 0$.

The main interest of the above construction in the case of a fixed family of discrete orientations $\mathcal{A} = \{\alpha_1, \dots, \alpha_N\}$ is that the resulting strength condition will be anisotropic with larger strength in the corresponding directions. We therefore expect the strength-based topology optimization procedure to naturally result in designs locally oriented in one of these directions.

By way of illustration, Figure 2 displays the uniaxial tensile strength in direction $\mathbf{e}_\theta = \cos \theta \mathbf{e}_x + \sin \theta \mathbf{e}_y$ for a material consisting of such a family of discrete orientations. As expected, when the reinforcement material is made of only two reinforcement directions, the material possesses no shear strength so that the uniaxial strength is always zero except if θ is perfectly aligned with one of the two directions. For more than two directions, the material possesses a shear strength and, therefore, a non-zero tensile strength for any θ . Again, we observe that the uniaxial strength is equal to f_t when the loading direction is aligned with one of the reinforcement direction and is less than f_t in-between. The resulting material therefore possesses anisotropic strength properties. In the limit of an isotropic continuous distribution of reinforcement direction, the uniaxial strength becomes a constant equal to f_t since the resulting material strength properties are equivalent to an isotropic L_1 -Rankine strength criterion.

4 Bi-material optimization

In this section, we investigate the concurrent optimization of multiple materials in addition to a void phase (see Figure 1-right). For simplicity, we restrict here to the case of two materials only, although the proposed procedure can be easily generalized to n different materials. We denote the two materials by their phase index $i = 1, 2$. Each material possesses a corresponding strength criterion G^i and a pseudo-density $0 \leq \rho_i \leq 1$ which we aim at optimizing.

4.1 Bi-material strength condition

Similarly to the discussion of section 3.4, we aim here at enforcing that a given point \mathbf{x} belongs to either phase 1 or phase 2. In terms of strength conditions, we would therefore have $\boldsymbol{\sigma} \in G^1$ or $\boldsymbol{\sigma} \in G^2$ which can be written as follows:

$$\exists \tilde{\boldsymbol{\sigma}}^1, \tilde{\boldsymbol{\sigma}}^2, \zeta_1, \zeta_2 \text{ s.t.} \quad \begin{cases} \boldsymbol{\sigma} = \zeta_1 \tilde{\boldsymbol{\sigma}}^1 + \zeta_2 \tilde{\boldsymbol{\sigma}}^2 \\ \tilde{\boldsymbol{\sigma}}^1 \in G^1 \\ \tilde{\boldsymbol{\sigma}}^2 \in G^2 \\ \zeta_1 + \zeta_2 = 1 \\ \zeta_1, \zeta_2 \in \{0, 1\} \end{cases} \quad (15)$$

where the binary variables ζ_i indicate the membership to the corresponding phase, the constraint $\zeta_1 + \zeta_2 = 1$ enforcing that either $\zeta_1 = 1, \zeta_2 = 0$ or $\zeta_1 = 0, \zeta_2 = 1$.

Again, this criterion is not convex due to the last binary constraint. As a result, we consider instead the tightest convex relaxation given by:

$$\boldsymbol{\sigma} \in \text{conv}\{G^1, G^2\} \Leftrightarrow \exists \tilde{\boldsymbol{\sigma}}^1, \tilde{\boldsymbol{\sigma}}^2, \zeta_1, \zeta_2 \quad (16)$$

$$\text{s.t.} \quad \begin{cases} \boldsymbol{\sigma} = \zeta_1 \tilde{\boldsymbol{\sigma}}^1 + \zeta_2 \tilde{\boldsymbol{\sigma}}^2 \\ \tilde{\boldsymbol{\sigma}}^1 \in G^1 \\ \tilde{\boldsymbol{\sigma}}^2 \in G^2 \\ \zeta_1 + \zeta_2 = 1 \\ 0 \leq \zeta_1, \zeta_2 \leq 1 \end{cases}$$

which is the convex hull of G^1 and G^2 . We now interpret the ζ_i as the partial density ρ_i of each phase which will be considered as optimization variables with the following constraint on the total density $\rho = \rho_1 + \rho_2$:

$$\rho_1 + \rho_2 \leq 1 \quad (17)$$

Note that changing to the above inequality instead of the equality constraint enables to model the occurrence of a void phase where $\rho_1 = \rho_2 = 0$.

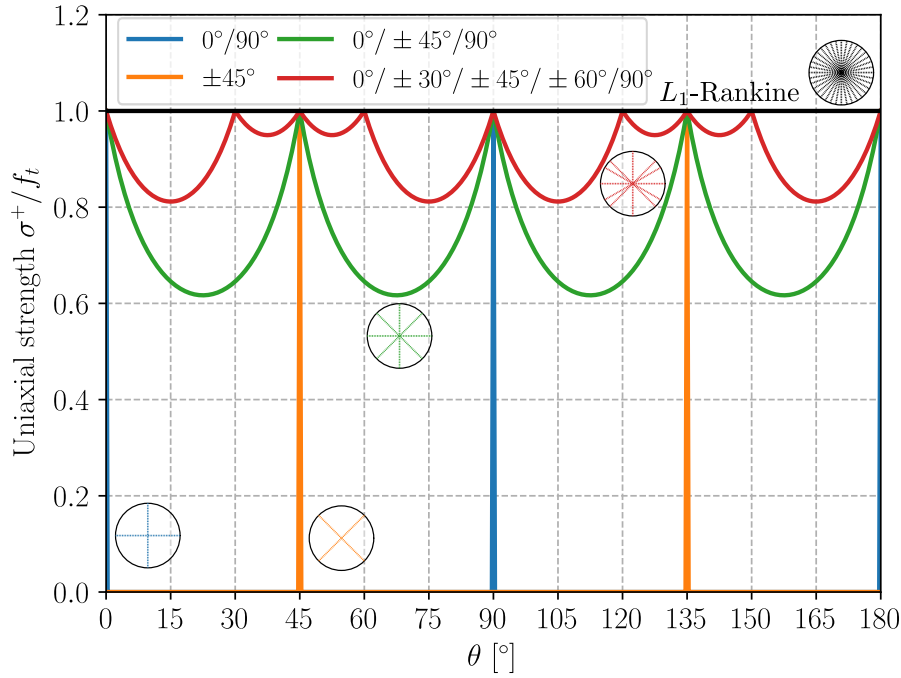


Fig. 2: Anisotropic uniaxial tensile strength for a material reinforced by a family of reinforcements of discrete orientations

We therefore consider from now on the following density-dependent strength condition $G(\rho_1, \rho_2)$ given by:

$$\sigma \in G(\rho_1, \rho_2) \Leftrightarrow \exists \sigma^1, \sigma^2 \text{ s.t. } \begin{cases} \sigma = \sigma^1 + \sigma^2 \\ \sigma^1 \in \rho_1 G^1 \\ \sigma^2 \in \rho_2 G^2 \end{cases} \quad (18)$$

in which we made the change of variable $\sigma^i = \rho_i \tilde{\sigma}^i$.

In particular, if both $\rho_1(\mathbf{x}) = \rho_2(\mathbf{x}) = 0$ at a given point \mathbf{x} , we have $\sigma(\mathbf{x}) = 0$ i.e. \mathbf{x} is in a void phase. If $\rho_1(\mathbf{x}) = 1$, then $\rho_2(\mathbf{x}) = 0$ and $\sigma(\mathbf{x}) \in G^1$ i.e. \mathbf{x} belongs to material 1 and vice versa. Note that it is possible to find states where $\rho_1(\mathbf{x}) \neq 0$ and $\rho_2(\mathbf{x}) \neq 0$ which results in \mathbf{x} belonging to a fictitious material averaging the strength properties of both phases.

Finally, in the case where $G^1 = G^2 = G$, we have $G(\rho_1, \rho_2) = (\rho_1 + \rho_2)G = \rho G$ and we recover the single material formulation of [30].

4.2 Convex problem formulation

The two corresponding load-maximization (LOAD-MAX) and volume minimization (VOL-MIN)

problems are therefore respectively given by:

$$\begin{aligned} \lambda^+ = \max_{\lambda, \sigma^1, \sigma^2, \rho_1, \rho_2} \quad & \lambda \\ \text{s.t.} \quad & \text{div}(\sigma^1 + \sigma^2) = 0 \quad \text{in } \mathcal{D} \\ & (\sigma^1 + \sigma^2) \cdot \mathbf{n} = \lambda \mathbf{T} \quad \text{on } \partial \mathcal{D}_T \\ & \sigma^1 \in \rho_1 G^1 \quad \text{in } \mathcal{D} \\ & \sigma^2 \in \rho_2 G^2 \quad \text{in } \mathcal{D} \\ & \int_{\mathcal{D}} c_\omega(\rho_1, \rho_2) \, dx \leq \eta |\mathcal{D}| \\ & 0 \leq \rho_1 \leq 1 \\ & 0 \leq \rho_2 \leq 1 \\ & \rho_1 + \rho_2 \leq 1 \end{aligned} \quad (\text{BIMAT-LOAD-MAX})$$

and

$$\begin{aligned} \eta^- = \min_{\sigma^1, \sigma^2, \rho_1, \rho_2} \quad & \frac{1}{|\mathcal{D}|} \int_{\mathcal{D}} c_\omega(\rho_1, \rho_2) \, dx \\ \text{s.t.} \quad & \text{div}(\sigma^1 + \sigma^2) = 0 \quad \text{in } \mathcal{D} \\ & (\sigma^1 + \sigma^2) \cdot \mathbf{n} = \lambda \mathbf{T} \quad \text{on } \partial \mathcal{D}_T \\ & \sigma^1 \in \rho_1 G^1 \quad \text{in } \mathcal{D} \\ & \sigma^2 \in \rho_2 G^2 \quad \text{in } \mathcal{D} \\ & 0 \leq \rho_1 \leq 1 \\ & 0 \leq \rho_2 \leq 1 \\ & \rho_1 + \rho_2 \leq 1 \end{aligned} \quad (\text{BIMAT-VOL-MIN})$$

where we introduced $c_\omega(\rho_1, \rho_2) = 2\omega\rho_1 + 2(1-\omega)\rho_2$ which is a weighted-average cost function measuring the

amount of both materials. As it will be seen later, the introduction of the weighting factor $\omega \in [0; 1]$ gives us increased flexibility in obtaining various optimal design depending on the cost associated with the presence of material 1 over material 2. Note that the above choice gives $c_{1/2}(\rho_1, \rho_2) = \rho_1 + \rho_2 = \rho$.

4.3 No-tension and no-compression materials

An important case of application of the previous bi-material formulation is concerned with the optimization of a no-tension and a no-compression phase. Practically, this could correspond to two different materials respectively possessing negligible tensile strength (e.g. concrete, rocks, masonry, etc.) and negligible compressive strength (e.g. thin membrane which would buckle under compression). Another possibility is to consider a single material for which we would like to distinguish members in tension from members in compression in the optimization process, for example in order to assign a different cost between the tensile and compressive "phase".

As regards this last point of view for a single material of nominal strength properties G , one could define the no-tension strength criterion $G^1 = G^- = G \cap S^-$ and the no-compression strength criterion $G^2 = G^+ = G \cap S^+$ where:

$$S^\pm = \{\boldsymbol{\sigma} \text{ s.t. } \pm \boldsymbol{\sigma} \succeq 0\} \quad (19)$$

represents the cone of symmetric positive/negative stress tensors. In this case, since $G^\pm \subset G$ and G is convex, we have that $\text{conv}\{G^+, G^-\} \subseteq G$. Again, this formulation will tend to promote stress states either in pure tension or in pure compression. Figure 3 illustrates this construction in the case of a Rankine and L_1 -Rankine criterion. Note that we have that $\text{conv}\{G^+, G^-\} = G^{L_1\text{-Rankine}}$ in this latter case.

Finally, as already discussed, the use of a L_1 -Rankine strength criterion will even further promote uniaxial stress states. If the original material is isotropic and possesses a characteristic tensile strength f_t and compressive strength f_c , a natural modeling strategy for obtaining truss-like designs when distinguishing the optimization of tensile and compressive members is therefore to consider:

$$G^1 = G^{L_1\text{-Rankine}(f_c, 0)} \quad (20)$$

$$G^2 = G^{L_1\text{-Rankine}(0, f_t)} \quad (21)$$

where $G^{L_1\text{-Rankine}(f_c, f_t)}$ denotes the isotropic L_1 -Rankine strength criterion of compressive (resp. tensile) strength f_c (resp. f_t).

Finally, the above choice can also be adapted to the situations for which members are constrained to have fixed potential orientations by using criteria of the form (12) instead of the isotropic L_1 -Rankine criterion.

5 Illustrative applications

5.1 Numerical implementation and penalization procedure

Similarly to [30], the corresponding discrete optimization problems are formulated using the `fenics_optim` package [6, 7] which enables to couple the FEniCS finite-element software package [2, 25] with the Mosek conic optimization solver [29]. The equilibrium constraint is enforced weakly through the virtual work principle using a continuous \mathbb{P}^2 -Lagrange interpolation for virtual displacement fields. The pseudo density fields are discretized using a continuous \mathbb{P}^1 -Lagrange interpolation, see [30] for more details. Mesh dependency issues are removed by adding a slope-control constraint [34] for $\|\nabla \rho_i\|_2 \leq 1/\ell$ for all density fields. Finally, we also extend the continuation procedure penalizing intermediate densities proposed in [30] to the present case. More precisely, each convex strength constraint of the form $\boldsymbol{\sigma}^i = \rho_i G^i$ is replaced by a penalized power-law (non-convex) constraint $\boldsymbol{\sigma}^i = (\rho_i)^p G^i$ following ideas of the SIMP method [5]. At each iteration of the penalization procedure, the power-law is linearized around the current density estimate $\rho_{i,n}$ and the exponent is progressively increased from 1 to a maximum value $p_{\max} > 1$, see again [30] for more details.

5.2 Numerical examples objectives

In the following, we will investigate three different examples which will have the common goal of assessing the versatility of the proposed methodology. Each of them will analyze some specific features which can be considered at the modeling stage, namely:

- MBB beam example:
 - Analyze the "reinforcement optimization" formulation and assess the influence of the reinforcement strength criterion choice (in terms of overall shape or anisotropy) on the resulting design;
 - Analyze the "bi-material optimization" formulation and assess the influence of the strength criterion of one of the phases on the resulting design;

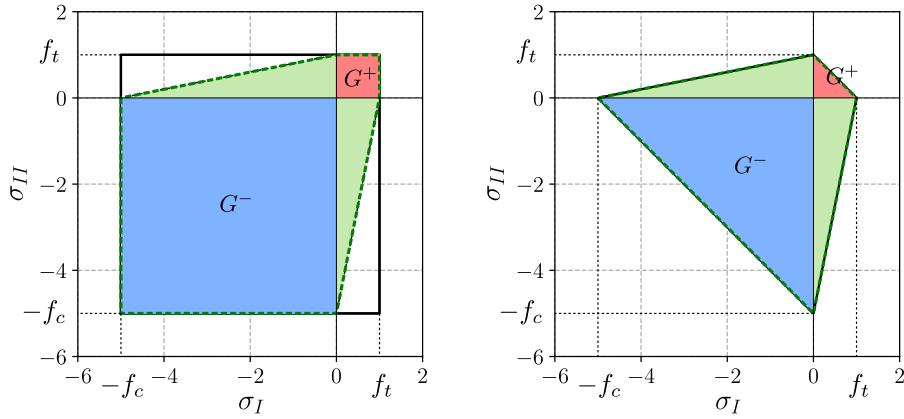


Fig. 3: Splitting of a nominal strength criterion G (in black) into a purely compressive part G^- (in blue) and a purely tensile part G^+ (in red) and the corresponding convex hull $\text{conv}\{G^+, G^-\}$ (in green). Left: a Rankine strength criterion, right: a L_1 -Rankine strength criterion in the plane of principal stresses

- Assess the corresponding formulation in which one phase only sustains tension and the other phase only compression;
- Assess the corresponding formulation where the tensile phase is subjected to a prescribed anisotropy in terms of reinforcement directions and compare its efficiency against an isotropic distribution of reinforcements.
- Bridge example:
 - Analyze the influence of asymmetric tensile and compressive strengths on the resulting design;
 - Compare the obtained design with a topology optimization involving a single material (with asymmetric strength properties);
 - Assess the influence of the cost function factor ω used to weight the cost of one phase with respect to another.
- Deep beam example:
 - Consider the design of widely studied reinforced concrete structure with an opening and compare the result against a strut-and-tie model used in practice;
 - Consider a variation in which the reinforcement phase can only be located in orthogonal directions;
 - Compare the designs obtained with the reinforcement and bi-material formulations.

5.3 MBB beam

We first consider a MBB beam example (Figure 4) of length $l = 36$ and height $h = 6$ with simple supports on the left and roller supports on the right, a vertical

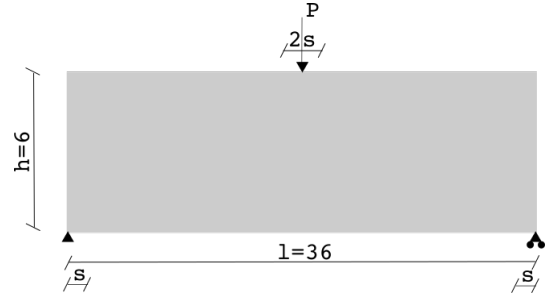


Fig. 4: A MBB beam example

force of reference intensity $P = 1$ is applied at the top. In the following, only one half of the model will be represented, taking symmetry into account. Both supports and force are distributed over a small distance $s = 0.5$ to mitigate stress concentrations. The mesh consists of approximately 40,000 elements.

5.3.1 Reinforcement optimization

We first consider the case of a fixed matrix material of strength condition G^m being given by a Rankine criterion of compressive strength $f_c^m = 1$ and tensile strength $f_t^m = 0.05$. The reinforced material effective strength criterion $G^{r,\text{eff}}$ will either be:

- a plane stress von Mises criterion with uniaxial tension/compression effective strengths $f_c^{r,\text{eff}} = f_t^{r,\text{eff}} = 1$
- a L_1 -Rankine criterion with the same uniaxial strengths
- a "no-compression" L_1 -Rankine criterion with $f_c^{r,\text{eff}} = 0$, $f_t^{r,\text{eff}} = 1$

- an orthotropic L_1 -Rankine criterion with $f_{tx}^{r,\text{eff}} = f_{ty}^{r,\text{eff}} = 1$ and $f_{cx}^{r,\text{eff}} = f_{cy}^{r,\text{eff}} = 0$

We consider the reinforcement load-maximization problem (REINF-LOAD-MAX) with an imposed volume fraction $\eta = 0.2$.

Figure 5 displays the obtained optimized reinforcement density in black along with the principal compressive stress field in the matrix phase in blue. Owing to the fact that the matrix phase has a low tensile strength, reinforcements are primarily located on the bottom tensile face of the beam. The amount of reinforcement increases from the support to the beam mid-span where the bending moment is maximum. The choice of the reinforcement phase strength criterion mainly influences small details in the layout such as the precise location of the reinforcements. The use of a von Mises criterion (Fig. 5a) for the reinforcement phase tends to favor biaxial stress states in the reinforcement region whereas the use of a L_1 -Rankine criterion (Fig. 5b) effectively promotes uniaxial stress states. Inclined reinforcements are also obtained to provide anchoring between the reinforcement tensile stress and the diffuse matrix compressive stresses. Moreover, when the reinforcement material possesses a non-zero compressive strength, we obtain a small amount of reinforcement on the top face at mid-span, thereby reinforcing the beam bending capacity. This region disappears in the case of a zero compressive strength (Fig. 5c). Finally, when considering an orthotropic L_1 -Rankine in Figure 5d, we obtain a 90°-bend as commonly encountered in reinforced-concrete structures.

5.3.2 Bi-material optimization

We now investigate the bimaterial load-maximization problem (BIMAT-LOAD-MAX) with again $\eta = 0.2$ and $\omega = 1/2$.

As in section 5.3.1, phase 1 corresponds to a Rankine criterion with $f_c = 1, f_t = 0.05$ and phase 2 with either a plane stress von Mises or a L_1 -Rankine criterion of strengths $f_c = f_t = 1$. Note that we voluntarily used similar compressive strengths for both phases. Figure 6 represents the optimized two phase densities in both cases. We can see that phase 1, with low tensile strength, is mostly used where it is the most efficient i.e. in the top part of the structure subjected to compression. The second phase is used mainly in tensile regions, except for the loading region in Figure 6a. This can be explained by the fact that this region is essentially under a biaxial compressive state, a stress state for which the von Mises criterion is larger than the Rankine criterion of phase 1. Let us also remark that the use of

a L_1 -Rankine criterion seems to yield a simpler design than that obtained with the von Mises material which can probably be attributed to the former promoting more efficiently uniaxial states.

Moreover, we can also observe in Figure 6 a transition between phase 1 and phase 2 materials along the inclined struts in compression on the right of the structure. This can be explained by the fact that we used the same uniaxial compressive strength f_c for both phases. Both of them are therefore equally optimal for uniaxial compression. The precise location of the transition between both phases is probably dictated by the initial distribution of the phase density in the initial stages of the penalization procedure. In such stages, phase 1 material is essentially located on the top part of the beam and phase 2 on the bottom part. The penalization process being a continuation procedure, it will naturally converge to a uniaxial stress state corresponding to the phase which was active initially. Note that the use of a phase 1 material with a lower compressive strength, e.g. $f_c = 0.9$ would have resulted in a design involving only phase 2 material, since phase 1 would have been strictly weaker and, therefore, less efficient than phase 2. In this case, the formulation becomes equivalent to a single-material formulation.

5.3.3 Splitting between tension and compression

We now investigate the formulation discussed in section 4.3 where phase 1 (resp. phase 2) corresponds to a pure compression (resp. pure tension) phase of strength f_c (resp. f_t). In practice, we use a L_1 -Rankine strength criterion for both phases with a small residual tensile (resp. compression) strength in phase 1 (resp. phase 2) to avoid numerical instabilities. Figure 7 represents the corresponding optimized densities for both phases and various imposed volume fractions η . Comparing for instance Figure 7c with Figure 6b, we can see that both final designs are very similar but with a different repartition between both phases. In the present tension/compression splitting formulation (21), each truss member belongs to a single phase, depending on its state of tension and compression whereas, in the previous formulation, some compression members could involve the phase 2 material or even both materials as already discussed.

5.3.4 Anisotropic strength properties for the tensile phase

We finish this example by considering again a tension/compression splitting formulation, except that the tensile phase (phase 2) now enjoys anisotropic strength

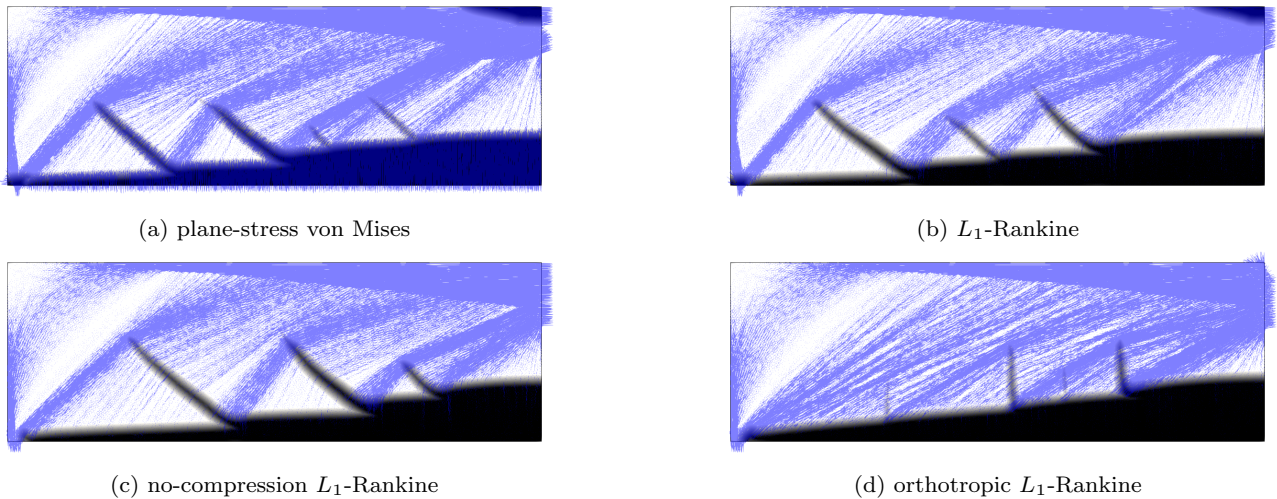


Fig. 5: Reinforcement optimization of the MBB example for various reinforcement strength criteria: in black, reinforcement optimized density; in blue, principal compressive stress in the matrix phase.

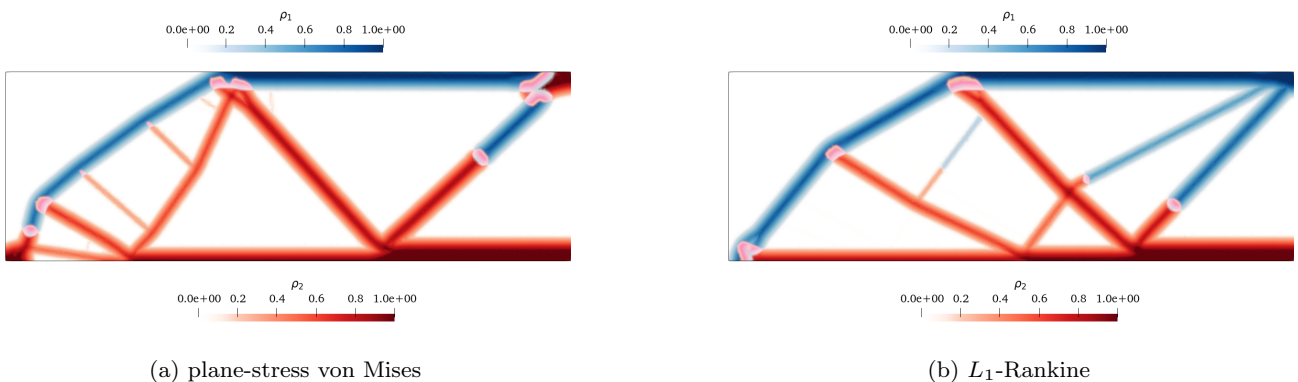


Fig. 6: Bi-material load-maximization of the MBB example: in blue, phase 1 density; in red, phase 2 density

properties of the form (12) with here $f_c^{r, \text{eff}} = 0$ and $f_t^{r, \text{eff}} = 1$. We recall that if the set of allowed orientations \mathcal{A} spans all directions, then the corresponding strength criterion is equivalent to a L_1 -Rankine strength criterion so that we recover the results of Figure 7. In Figure 8, we report the results obtained when considering a tensile phase with allowed orientations of $\alpha = 0^\circ$, $\alpha \in \{0^\circ; \pm 30^\circ\}$, $\alpha \in \{0^\circ; \pm 45^\circ\}$ or $\alpha \in \{0^\circ; 90^\circ\}$. As expected, if tensile members can be aligned horizontally only (Figure 8a), the most efficient design is obtained with tensile members located at the bottom of the beam and with inclined compressive struts transmitting the load to the supports. Interestingly, we obtain two individual tensile members in this case. When we further allow for inclined directions along $\pm 30^\circ$ or $\pm 45^\circ$, we obtain, in addition to a horizontal tensile member, secondary inclined mem-

bers to which additional compressive struts can be connected. Note that the case $\alpha \in \{0^\circ; \pm 45^\circ\}$ (Figure 8c) is quite close to the isotropic case obtained with the L_1 -Rankine criterion in Figure 7c. Finally, the case with $\alpha \in \{0^\circ; 90^\circ\}$ (Figure 8d) indeed produces tensile members aligned either horizontally or vertically. Interestingly, despite the fact that tensile orientations are constrained, one still has freedom in the length and location of those members which enables to reach a design where compressive struts can more or less follow the same paths as in the isotropic case. Also note that the convexified formulation (12) authorizes in theory a superposition of the different orientations at a given point. Clearly, this is not observed since each tensile member is in a pure uniaxial stress state corresponding to a single well-defined orientation. It is only at points corresponding to junctions between tensile and/or com-

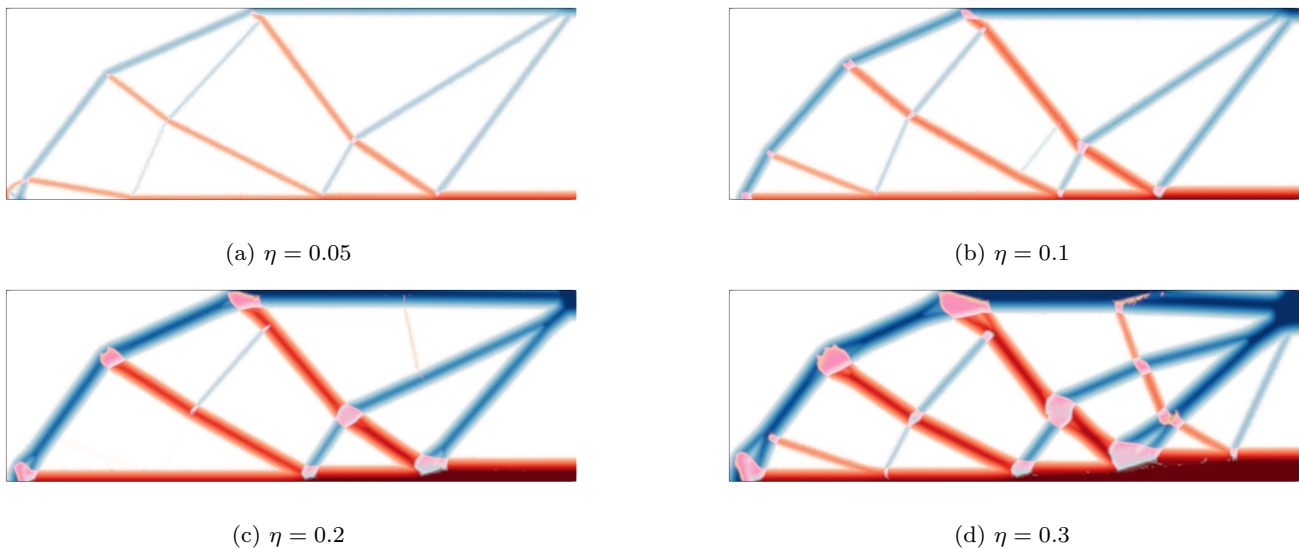


Fig. 7: Bi-material load-maximization of the MBB example with tension/compression splitting ($f_c = f_t = 1$) and various maximum volume fraction η

pressive members that different orientations may coexist.

Figure 9 compares the corresponding load-bearing capacity of the previous discrete orientation designs with that of the isotropic case. As expected, the isotropic case is the most efficient in terms of load-bearing capacity, both at the beginning and at the end of the penalization procedure. The case with only horizontal tensile members is the less efficient whereas the case with 45° shows only slightly lower bearing capacity than the isotropic case which can be explained by the fact that the corresponding design was already quite close to that of the isotropic case.

5.4 Bridge example

We now turn to a bridge-like problem as described in Figure 10. On this example, we investigate the influence of asymmetric tensile/compressive strengths. We again use load-maximization formulations with $\eta = 0.2$ for the imposed volume fraction and $\omega = 1/2$. In particular, figures 11, 12 and 13 compare the obtained optimized design when using either a bi-material or a single material formulation in the cases where $f_c = f_t = 1$, $f_c = 1$, $f_t = 10$ and $f_c = 10$, $f_t = 1$ respectively. As expected, we observe relatively similar designs from the two formulations in terms of general layout of members in tension and compression. Nevertheless, small differences can be observed, especially on Figure 12. Such differences can be attributed to the fact that the bi-material formulation treats differently the behavior

of connections between tension and compression members compared to the single material formulation. One can in particular observe that such connections have a larger spatial extension in the bi-material case. Indeed, in locations where both tension and compression phases coexist, the bi-material formulation allows for reduced strength properties compared to the single material phase. For instance, if $\rho_1 = \rho_2$, then at most $\rho_1 = \rho_2 = 0.5$ such that the effective tension and compression strengths are here $f_c/2$ and $f_t/2$, that is half of that of the single material formulation which can reach full capacity. This modeling aspect reflects the fact that anchoring two different materials usually has a detrimental effect on the local strength compared to a single material possessing both tensile and compressive strengths.

Although, the single material formulation of [30] enables to obtain similar design as the bi-material formulation, the latter has the advantage of offering additional modeling choices by using a different factor in the combined volume measure of both phases through the factor ω . For instance, Figure 14 represents the evolution of the obtained design when varying this weighting coefficient. We can see that when $\omega < 0.5$, tensile (phase 2) material costs more than compression (phase 1) material. The number of tensile members therefore tends to decrease with decreasing ω . It must be noted that, although compressive members seem slightly thicker, the number of such members do not necessarily increase with decreasing tensile material since they still need to be connected with tensile members to be supported.

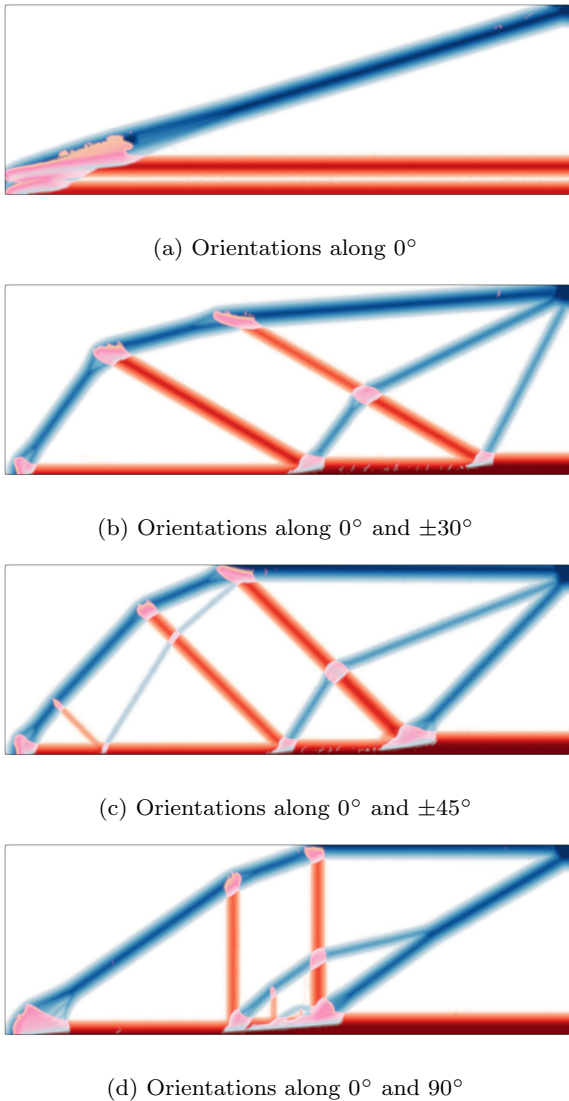


Fig. 8: Bi-material load-maximization ($\eta = 0.2$) of the MBB example with discrete orientations for the tensile phase

Conversely, when ω increases above the value 0.5, tensile members cost less than compression members and can therefore be utilized more extensively. Figure 15 represents the evolution of the structure load-bearing capacity as a function of the penalization procedure iterations for the considered values of ω . Interestingly, the initial value corresponding to the convex problem (BIMAT-LOAD-MAX) does not strongly depend on the density cost parameter ω . However, during the penalization procedure, the choice of ω leads to different optimized designs, some of which performing better than other in terms of bearing capacity. In particular, the case $\omega = 0.9$ yields a more efficient structure which may

be explained by the fact that more tensile material can be considered since it costs less in terms of weighted volume than compressive material.

5.5 Deep beam example

We now finish with a deep beam example classically considered when dealing with the design of massive reinforced concrete structures, see Figure 16. Such structures offer great challenges to engineers when aiming at proposing an efficient reinforcement steel layout. Many solutions are possible in practice, depending on the priority given to the simplicity of the design (number of members, orientations, etc.) or to its optimality in terms of steel consumption for instance. In this section, we show how our methodology can easily address both concerns.

With the proposed methodology we consider a total design load $Q = 2$ MN and formulate a bimaterial volume minimization problem. The first phase, representing concrete is modeled with a L_1 -Rankine criterion with $f_c = 40$ MPa and $f_t = 0.1$ MPa, the second phase, representing steel rebar reinforcements, is modeled with a L_1 -Rankine criterion with (almost) no compressive strength and an effective tensile strength $f_t = \chi f_y = 40$ MPa where $f_y = 400$ MPa is the steel tensile strength and $\chi = 0.1$ a strength reduction factor accounting for the fact that, in practice, steel rebars only occupy a small fraction (10% at maximum in the present case) of the total beam thickness. Both phases have identical volume cost ($\omega = 0.5$) and we use $\ell = 0.15$.

Figure 17a represents the obtained design for both phases. We can clearly see multiple compressive struts aiming at the beam supports, equilibrated by a bottom horizontal tensile reinforcement and a more complex curved reinforcement above the beam opening. Clearly the obtained design is quite similar to strut-and-tie models proposed in [31] based on elastic stress fields, see Figure 17b. The global structural behavior in terms of strut and tie location is quite similar between both models. There are however some noticeable differences: since the ST model of Figure 17b is based on the interpretation of elastic stress fields, the two main compressive struts exhibit a characteristic "bottle" shape corresponding to the diffusion of elastic stress fields between singular points corresponding to point loads and supports. Such a diffusion induces the presence of small secondary transverse reinforcements which help preventing cracking of concrete in tension. Such features are typical of elastic computations and are therefore absent from limit-analysis based computation which yield very straight compressive struts with constant cross-section.

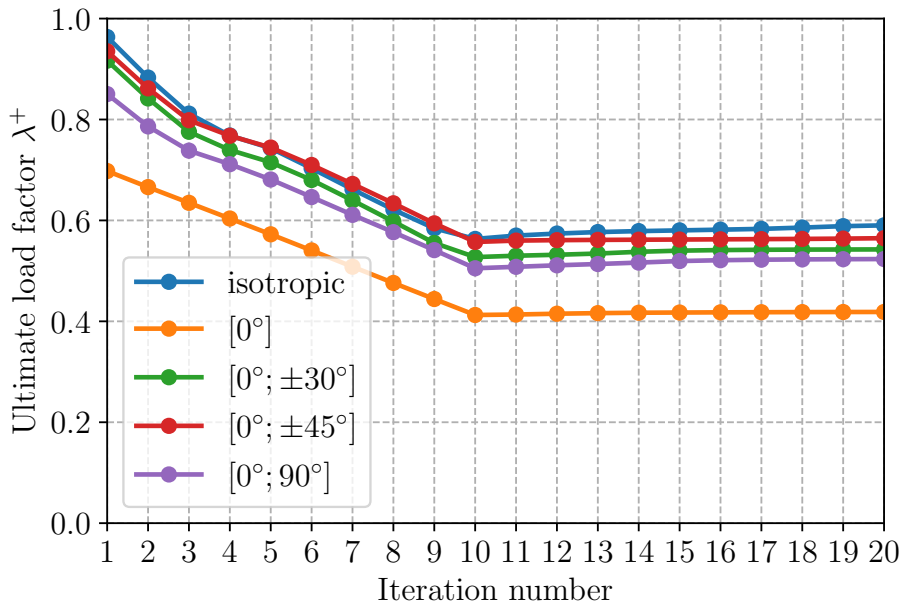
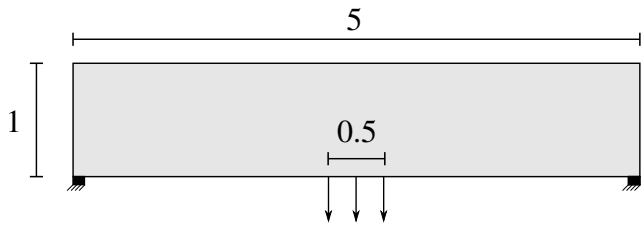


Fig. 9: Evolution of the load-bearing capacity during the penalization procedure for the MBB example with discrete tensile orientations

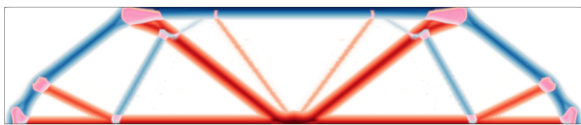


(a) bi-material



(b) single material

Fig. 10: A bridge structure with a central uniformly distributed loading $\mathbf{T} = -\mathbf{e}_y$. Fixed supports are distributed over regions of length 0.1 at both extremities.



(a) bi-material



(b) single material

Fig. 11: Symmetric strengths $f_c = f_t = 1$

Fig. 12: Asymmetric strengths $f_c = 1, f_t = 10$



(a) bi-material



(b) single material

Fig. 13: Asymmetric strengths $f_c = 10, f_t = 1$

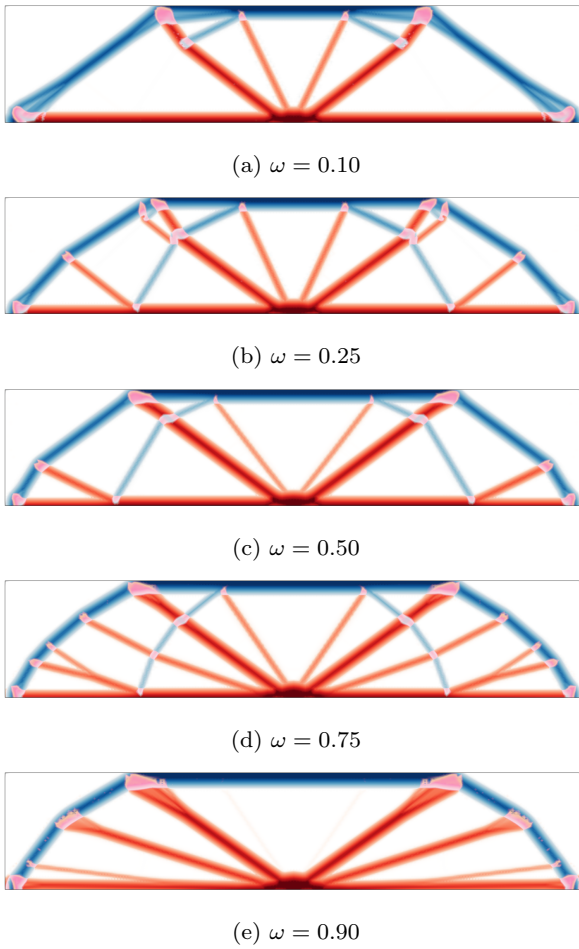


Fig. 14: Bridge example with varying density-cost parameter ω in the case $f_c = f_t = 1$

Similarly, we can note that the "array" of struts emerging from the point load is much wider in the ST model than what is obtained with our procedure, for similar reasons.

As pointed out above, such a complex rebar layout might not be practical for on-site placing for instance. Engineers therefore aim at obtaining simpler solutions, although being less optimal, which might be easier to implement in practice. A typical simplifying choice in the design of reinforced concrete structures is to resort to orthogonal reinforcement layout. To achieve this, we simply modify the isotropic strength criterion of the tensile phase with an orthotropic criterion with admissible reinforcement orientations of 0° or 90° . The corresponding result is represented in Figure 18a which indeed results in steel rebars being either placed horizontally or vertically. Again, the obtained design is compared with a ST model including only horizontal or vertical reinforcements in Figure 18b. We can again notice

the striking similarity between both models with some differences in terms of steel rebar lengths for instance.

Similarly, the reinforcement optimization formulation where the concrete is not optimized has also been considered on the same example. Results are reported on Figure 19 for both the L_1 -Rankine and orthotropic L_1 -Rankine criterion for the reinforcement phase. Clearly, this formulation provides reinforcement layouts qualitatively similar to the bi-material case. We can notice that the amount of reinforcement is however much less than in Figures 17a and 18a since, in the present case, concrete strength can be mobilized in the whole computational domain, thereby requiring less reinforcement to sustain the same load. However, the concrete stress field is still well localized and compressive concrete struts can be observed. This observation is interesting since the reinforcement optimization formulation involves only a single density variable and is therefore much less computationally intensive than the bi-material formulation.

6 Conclusions, discussion and future work

This work proposed an extension of limit analysis-based topology optimization problems to the case of multiple materials. In particular, the structural load-bearing capacity can be maximized under a material cost constraint. Alternatively, the total material cost function can be minimized for a given imposed loading. Following similar numerical techniques (penalization procedure, filtering) as a previous contribution dedicated to a single material [30], the main contribution of the present work is related to the way composite materials are represented.

We first proposed a reinforcement formulation, in which we aim at optimizing only a reinforcement phase (e.g. steel rebars, fibers, etc.) embedded in a fixed background matrix material (e.g. concrete, soil, resin, etc.). The chosen strength criterion for the reinforcement phase attempts at promoting uniaxial stress states. Reinforcements can be either isotropically distributed (using the L_1 -Rankine criterion) or with fixed preferential orientation directions (anisotropic criterion (12)).

Second, we proposed a formulation in which two distinct material phases are simultaneously optimized, each of them possessing its own distinct strength criterion. The latter can either be an isotropic one or an anisotropic one such as (12). Each phase can also represent either two intrinsically distinct materials or represent instead a fictitious phase with a specific stress state, e.g. pure tension and pure compression as in section 4.3. The introduction of a material cost function $c_\omega(\rho_1, \rho_2)$ also enables to consider a different

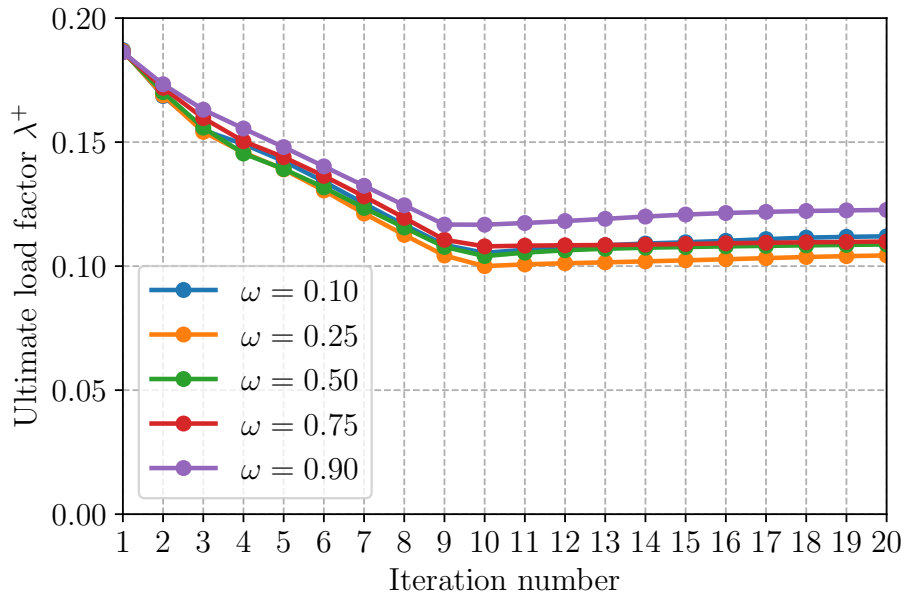


Fig. 15: Evolution of the load-factor during the penalization procedure for various cost parameters

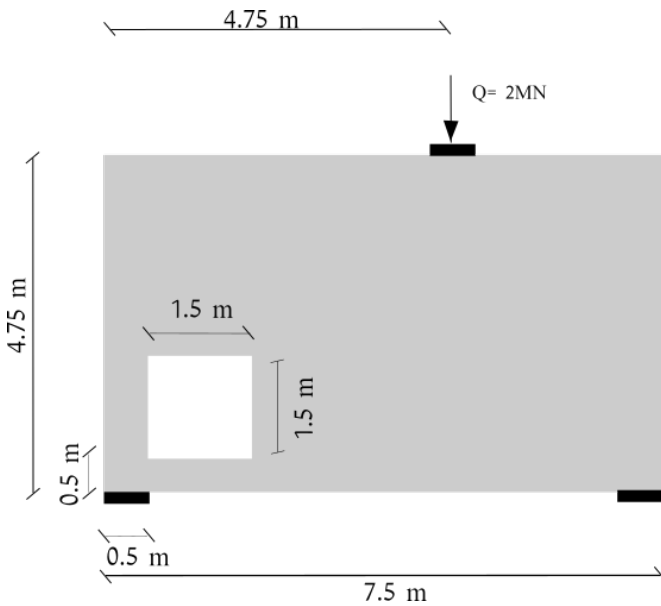


Fig. 16: Deep beam problem (25 mm thick) investigated in [31]

cost for each phase through the weighting coefficient ω . All these possibilities make the proposed formulation extremely versatile in terms of modeling capabilities.

The question remains which of the reinforcement or bimaterial formulation is more appropriate. Obviously, there is no definitive answer as it depends on

the targeted application and the potential need for exploring different topologies. Let us first say that the reinforcement formulation can be seen as a particular case of the bimaterial formulation in which one of the phase pseudo-density is fixed to a value of 1 and where the constraint $\rho_1 + \rho_2 \leq 1$ is ignored. The bimaterial formulation is, in this respect, more general but is also much more computationally demanding as two phases must be optimized instead of one. Second, considering a fixed background phase occupying the whole domain produces much more diffuse matrix stress fields in some instances (see Fig. 5). For some applications such as the strut-and-tie method for reinforced concrete structures, it might be more interesting to have a clear and simplified stress field in the concrete phase, despite the fact that concrete still occupies the whole structure. In such cases, the bi-material formulation seems particularly attractive. Finally, the latter approach also offers a richer way of exploring various topologies through the choice of the phase criteria or the weighting cost factor.

As regards future works, the possibility of generating strut-and-tie models with the proposed formulation seems very promising. It remains to be checked that the obtained models qualitatively agree with engineering practice on a wider range of examples. One should also check that the corresponding internal forces also quantitatively agree with calculations based on Eurocode design norms. Finally, as the proposed bi-material for-

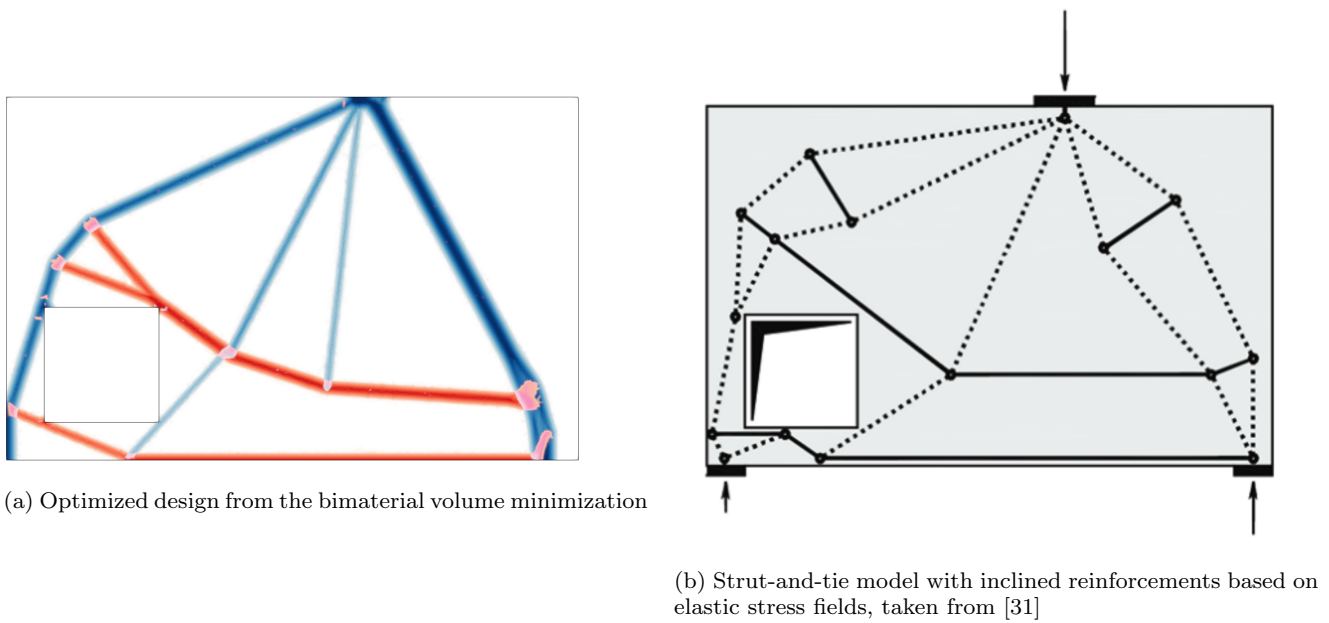


Fig. 17: Comparison of the proposed methodology with strut-and-tie models with inclined reinforcements

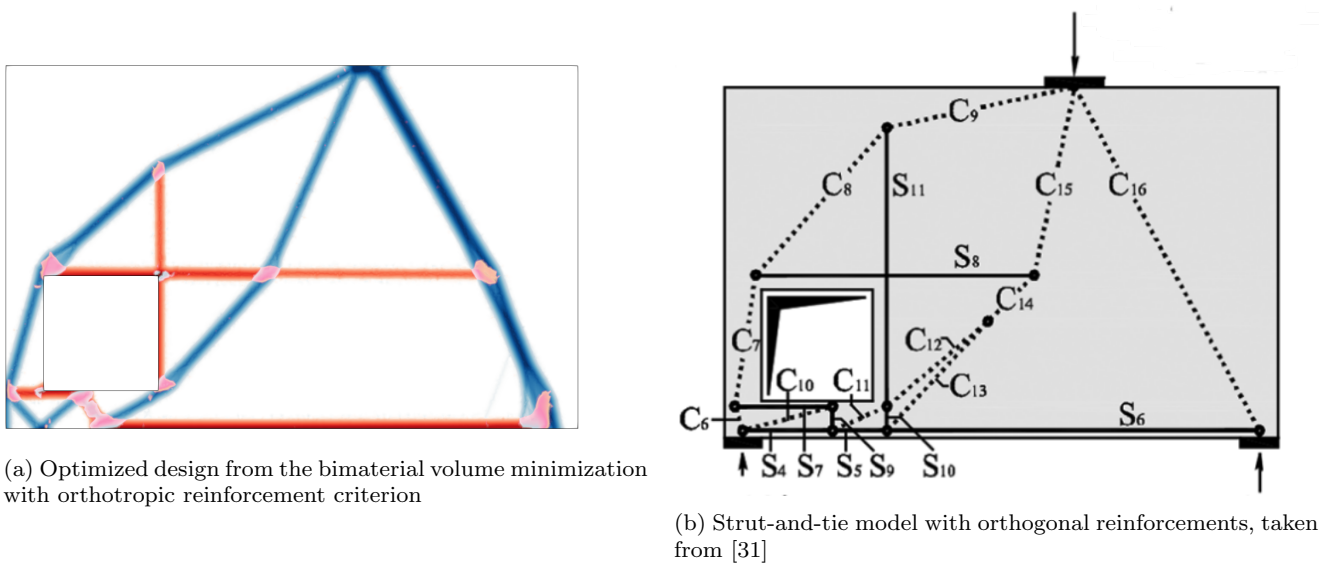


Fig. 18: Comparison of the proposed methodology with strut-and-tie models with orthogonal reinforcements

mulation is computationally demanding, its extension to 3D would require developing dedicated numerical strategies in order to reduce its computational cost.

Conflict of interest

The authors declare that they have no conflict of interest.

Replication of results

The Python code for implementing the topology optimization is part of the `fenics_optim` Python package (v2.0) [7], itself relying on the FEniCS finite-element software library <https://fenicsproject.org/> and the Mosek conic optimization solver <https://www.mosek.com/>.

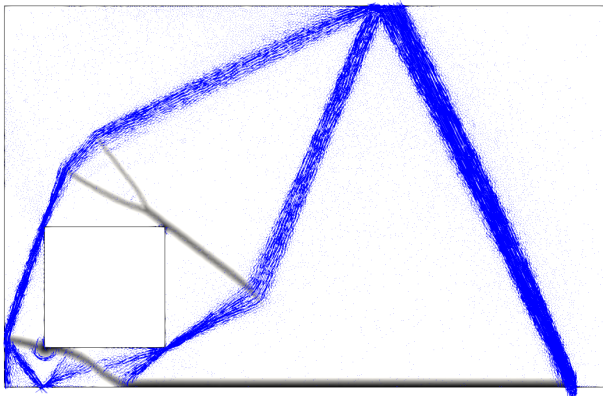
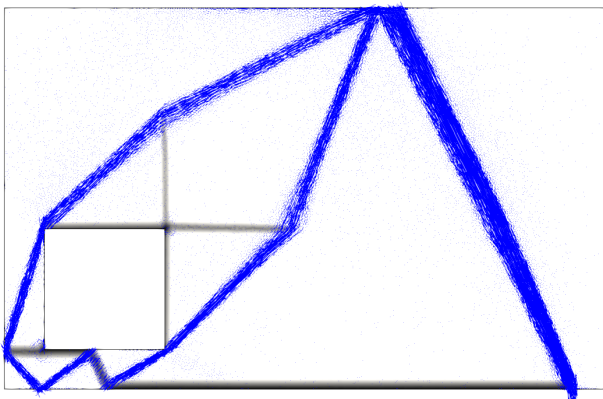
(a) L_1 -Rankine criterion(b) orthotropic L_1 -Rankine criterion

Fig. 19: Reinforcement optimization of the deep beam example: in black, reinforcement optimized density; in blue, principal compressive stress in the matrix phase

References

- Allaire, G., Dapogny, C., Delgado, G., Michailidis, G.: Multi-phase structural optimization via a level set method. *ESAIM: control, optimisation and calculus of variations* **20**(2), 576–611 (2014)
- Alnæs, M.S., Blechta, J., Hake, J., Johansson, A., Kehlet, B., Logg, A., Richardson, C., Ring, J., Rognes, M.E., Wells, G.N.: The fenics project version 1.5. *Archive of Numerical Software* **3**(100) (2015). DOI 10.11588/ans.2015.100.20553
- Amir, O.: Stress-constrained continuum topology optimization: a new approach based on elastoplasticity. *Structural and Multidisciplinary Optimization* **55**(5), 1797–1818 (2017)
- Amir, O., Bogomolny, M.: Conceptual design of reinforced concrete structures using topology optimization with elastoplastic material modeling. *International Journal for Numerical Methods in Engineering* **90**, 1578–1597 (2012). DOI 10.1002/nme.4253
- Bendsøe, M.P., Sigmund, O.: *Topology optimization: theory, methods, and applications*, 2. ed., corr. printing edn. Engineering online library. Springer (2004). OCLC: 249399186
- Bleyer, J.: Automating the formulation and resolution of convex variational problems: Applications from image processing to computational mechanics. *ACM Trans. Math. Softw.* **0**(ja) (2020). DOI 10.1145/3393881. URL <https://doi.org/10.1145/3393881>
- Bleyer, J.: fenics-optim – Convex optimization interface in FEniCS (2020). DOI 10.5281/zenodo.3604086. URL <https://doi.org/10.5281/zenodo.3604086>
- Bruggi, M.: Generating strut-and-tie patterns for reinforced concrete structures using topology optimization. *Computers & Structures* **87**, 1483–1495 (2009). DOI 10.1016/j.compstruc.2009.06.003
- Bruggi, M.: ANALYSIS AND DESIGN OF REINFORCED CONCRETE STRUCTURES AS a TOPOLOGY OPTIMIZATION PROBLEM. In: *Proceedings of the VII European Congress on Computational Methods in Applied Sciences and Engineering (ECCOMAS Congress 2016)*, pp. 3271–3279. Institute of Structural Analysis and Antiseismic Research School of Civil Engineering National Technical University of Athens (NTUA) Greece (2016). DOI 10.7712/100016.2033.5930. URL <http://www.eccomasproceedia.org/conferences/eccomas-congresses/eccomas-congress-2016/2033>
- Buhan, P.D., Taliercio, A.: A homogenization approach to the yield strength of composite materials. *European Journal of Mechanics A-solids* **10**, 129–154 (1991)
- Chavez, G.M.: *Strut-and-tie models for the design of non-flexural elements: computational aided approach*. Ph.D. thesis, Université Paris-Est (2018)
- Collins, M.P., Mitchell, D.: Shear and torsion design of prestressed and non-prestressed concrete beams. *J. Prestressed Concr. Inst.* pp. 25(5), 32–100 (1980)
- De Buhan, P., Bleyer, J., Hassen, G.: *Elastic, Plastic and Yield Design of Reinforced Structures*. Elsevier (2017)
- Dorn, W.: Automatic design of optimal structures. *J. de Mecanique* **3**, 25–52 (1964)
- Duysinx, P., Bendsøe, M.P.: Topology optimization of continuum structures with local stress constraints. *International journal for numerical methods in engineering* **43**(8), 1453–1478 (1998)

16. Fin, J., Borges, L., Fancello, E.: Structural topology optimization under limit analysis. *Structural and Multidisciplinary Optimization* **59** (2018). DOI 10.1007/s00158-018-2132-y
17. Gaynor, A.T., Guest, J.K., Moen, C.D.: Reinforced concrete force visualization and design using bilinear truss-continuum topology optimization. *Journal of Structural Engineering* **139**(4), 607–618 (2013). DOI 10.1061/(ASCE)ST.1943-541X.0000692. URL <http://ascelibrary.org/doi/10.1061/%28ASCE%29ST.1943-541X.0000692>
18. Gibiansky, L.V., Sigmund, O.: Multiphase composites with extremal bulk modulus. *Journal of the Mechanics and Physics of Solids* **48**(3), 461–498 (2000)
19. Gilbert, M., Tyas, A.: Layout optimization of large-scale pin-jointed frames. *Engineering computations* (2003)
20. Guest, J.: Topology optimization with multiple phase projection. *Computer Methods in Applied Mechanics and Engineering - COMPUT METHOD APPL MECH ENG* **199**, 123–135 (2009). DOI 10.1016/j.cma.2009.09.023
21. He, L., Gilbert, M.: Rationalization of trusses generated via layout optimization. *Structural and Multidisciplinary Optimization* **52**(4), 677–694 (2015)
22. Herfelt, M., Poulsen, P., Hoang, L.: Strength-based topology optimisation of plastic isotropic von mises materials. *Structural and Multidisciplinary Optimization* (2018). DOI 10.1007/s00158-018-2108-y
23. Kammoun, Z., Smaoui, H.: A direct approach for continuous topology optimization subject to admissible loading. *Comptes Rendus Mécanique* **342**(9), 520–531 (2014)
24. Liu, J., Ma, Y.: A new multi-material level set topology optimization method with the length scale control capability. *Computer Methods in Applied Mechanics and Engineering* **329**, 444–463 (2018)
25. Logg, A., Mardal, K.A., Wells, G.: Automated solution of differential equations by the finite element method: The FEniCS book, vol. 84. Springer Science & Business Media (2012)
26. Marti: On plastic analysis of reinforced concrete. Institute of Structural Engineers, ETH, Zurich, Switzerland (1980)
27. Maute, K., Schwarz, S., Ramm, E.: Adaptive topology optimization of elastoplastic structures. *Structural Optimization* **15**(2), 81–91 (1998). DOI 10.1007/BF01278493. URL <http://link.springer.com/10.1007/BF01278493>
28. Michell, A.G.M.: LVIII. The limits of economy of material in frame-structures. *The London, Edinburgh, and Dublin Philosophical Magazine and Journal of Science* **8**(47), 589–597 (1904)
29. MOSEK ApS, .: The MOSEK optimization API for Python 8.1.0 (2018). URL <http://docs.mosek.com/8.1/pythonapi/index.htm>
30. Mourad, L., Bleyer, J., Mesnil, R., Nseir, J., Sab, K., Raphael, W.: Topology optimization of load-bearing capacity. *Structural and Multidisciplinary Optimization* (2021)
31. Muttoni, A., Fernández Ruiz, M., Niketić, F.: Design versus assessment of concrete structures using stress fields and strut-and-tie models. *ACI Structural Journal* **112**(5) (2015). DOI 10.14359/51687710. URL <http://www.concrete.org/Publications/InternationalConcreteAbstractsPortal.aspx?m=details&i=51687710>
32. Mörsch, E., Goodrich, E.: Concrete-steel Construction: (Der Eisenbetonbau). Engineering News Publishing Company (1909)
33. Pedersen, P.: Some general optimal design results using anisotropic, power law nonlinear elasticity. *Structural Optimization* **15**(2), 73–80 (1998). DOI 10.1007/bf01278492. URL <https://link.springer.com/article/10.1007/BF01278492>
34. Petersson, J., Sigmund, O.: Slope constrained topology optimization. *International Journal for Numerical Methods in Engineering* **41**(8), 1417–1434 (1998)
35. Prager, W.: Introduction to structural optimization. Springer (1974)
36. Querin, O.M., Victoria, M., Martí, P.: Topology optimization of truss-like continua with different material properties in tension and compression. *Structural and Multidisciplinary Optimization* **42**(1), 25–32 (2010)
37. Ritter: Die bauweise hennebique (the hennebique system). *Schweizerische Bauzeitung*, Bd **XXXIII**, 7.2 (1899)
38. Rostami, P., Marzbanrad, J.: Multi-material topology optimization of compliant mechanisms using regularized projected gradient approach. *Journal of the Brazilian Society of Mechanical Sciences and Engineering* **42** (2020). DOI 10.1007/s40430-020-02549-2
39. Rozvany, G., Ong, T.: Optimal plastic design of plates, shells and shellgrids. In: *Inelastic behaviour of plates and shells*, pp. 357–384. Springer (1986)
40. Schlaich, J., Schafer, K., Jennewein, M.: Toward a consistent design of structural concrete. *PCI Journal* **32**(3), 74–150 (1987). DOI 10.15554/pci.05011987.74.150. URL http://www.pci.org/pci_journal-1987-may-june-5/

41. Sigmund, O., Torquato, S.: Design of materials with extreme thermal expansion using a three-phase topology optimization method. *Journal of the Mechanics and Physics of Solids* **45**(6), 1037–1067 (1997)
42. Smarslik, M., Ahrens, M.A., Mark, P.: Toward holistic tension-or compression-biased structural designs using topology optimization. *Engineering Structures* **199**, 109632 (2019)
43. Strang, G., Kohn, R.V.: Optimal design in elasticity and plasticity. *International journal for numerical methods in engineering* **22**(1), 183–188 (1986)
44. Swan, C.C., Kosaka, I.: Voigt-reuss topology optimization for structures with nonlinear material behaviors. *International Journal for Numerical Methods in Engineering* **40**(20), 3785–3814 (1997). DOI 10.1002/(SICI)1097-0207(19971030)40:20<3785::AID-NME240>3.0.CO;2-V. URL <http://doi.wiley.com/10.1002/%28SICI%291097-0207%2819971030%2940%3A20%3C3785%3A%3AAID-NME240%3E3.0.CO%3B2-V>
45. Tavakoli, R.: Multimaterial topology optimization by volume constrained allen-cahn system and regularized projected steepest descent method. *Computer Methods in Applied Mechanics and Engineering* **276** (2014). DOI 10.1016/j.cma.2014.04.005
46. Victoria Nicolás, M., Querin, O., Martí-Montrull, P.: Generation of strut-and-tie models by topology design using different material properties in tension and compression. *Structural and Multidisciplinary Optimization* **44**, 247–258 (2011). DOI 10.1007/s00158-011-0633-z
47. Wallin, M., Ivarsson, N., Ristinmaa, M.: Large strain phase-field-based multi-material topology optimization. *International Journal for Numerical Methods in Engineering* **104**(9), 887–904 (2015)
48. Wallin, M., Jönsson, V., Wingren, E.: Topology optimization based on finite strain plasticity. *Structural and multidisciplinary optimization* **54**(4), 783–793 (2016)
49. Zhang, X., Chi, H., Paulino, G.: Adaptive multi-material topology optimization with hyperelastic materials under large deformations: A virtual element approach. *Computer Methods in Applied Mechanics and Engineering* **370**, 112976 (2020). DOI 10.1016/j.cma.2020.112976
50. Zhang, X., Paulino, G., Ramos, A.: Multi-material topology optimization with multiple volume constraints: a general approach applied to ground structures with material nonlinearity. *Structural and Multidisciplinary Optimization* **57** (2018). DOI 10.1007/s00158-017-1768-3

51. Zhang, X.S., Paulino, G.H., Ramos, A.S.: Multi-material topology optimization with multiple volume constraints: a general approach applied to ground structures with material nonlinearity. *Structural and Multidisciplinary Optimization* **57**(1), 161–182 (2018)
52. Zhou, S., Wang, M.Y.: Multimaterial structural topology optimization with a generalized cahn–hilliard model of multiphase transition. *Structural and Multidisciplinary Optimization* **33**(2), 89 (2007)
53. Zuo, W., Saitou, K.: Multi-material topology optimization using ordered simp interpolation. *Structural and Multidisciplinary Optimization* **55** (2017). DOI 10.1007/s00158-016-1513-3

A Proof that the L_1 -Rankine criterion is the convex hull of isotropically distributed uniaxial strengths

Let us consider an infinite distribution of uniaxial reinforcements indexed by α with tensile and compressive strengths f_t and f_c (independent of α). Let us denote by $G^\alpha = \{\sigma_\alpha e_\alpha \otimes e_\alpha \text{ s.t. } -f_c \leq \sigma_\alpha \leq f_t\}$ the uniaxial strength criterion of a given family of reinforcement. We show that:

$$G^{L_1\text{-Rankine}} = \mathbf{conv}_\alpha \{G^\alpha\} \quad (22)$$

where $G^{L_1\text{-Rankine}}$ is the L_1 -Rankine criterion defined in (2) which can also be equivalently written as:

$$\sigma \in G^{L_1\text{-Rankine}} \Leftrightarrow \begin{cases} \sigma_I + \sigma_{II} \leq f_t \\ -\sigma_I - \sigma_{II} \leq f_c \\ \sigma_I/f_t - \sigma_{II}/f_c \leq 1 \\ -\sigma_I/f_c + \sigma_{II}/f_t \leq 1 \end{cases} \quad (23)$$

Note that although everything is written in a 2D setting, the following proof also holds in 3D.

Proof Let us first show that $G^{L_1\text{-Rankine}} \subseteq \mathbf{conv}_\alpha \{G^\alpha\}$. For any given stress tensor, we have $\sigma = \sigma_I e_I \otimes e_I + \sigma_{II} e_{II} \otimes e_{II}$. Then there exist two families of reinforcement α_I and α_{II} of respective orientation e_I and e_{II} . Moreover, assuming that $\sigma \in G^{L_1\text{-Rankine}}$ and introducing $\zeta_I = g(\sigma_I)$ and $\zeta_{II} = g(\sigma_{II})$, we have:

$$-f_c \leq \frac{\sigma_I}{\zeta_I} \leq f_t \quad (24)$$

$$-f_c \leq \frac{\sigma_{II}}{\zeta_{II}} \leq f_t \quad (25)$$

and $\zeta_I + \zeta_{II} \leq 1$. As a result, σ can indeed be written as (12) with $\sigma^{r,\alpha_I} = \sigma_I/\zeta_I$ and $\sigma^{r,\alpha_{II}} = \sigma_{II}/\zeta_{II}$ so that $G^{L_1\text{-Rankine}} \subseteq \mathbf{conv}_\alpha \{G^\alpha\}$.

Now let us show that $\mathbf{conv}_\alpha \{G^\alpha\} \subseteq G^{L_1\text{-Rankine}}$. Let σ given by (12). Let e_I and e_{II} be the principal stress

directions of this stress state and introduce θ_α such that $\mathbf{e}_\alpha = \cos \theta_\alpha \mathbf{e}_I + \sin \theta_\alpha \mathbf{e}_{II}$ for any α . Then:

$$\sigma_I = \sum_{\alpha} \zeta_{\alpha} \cos^2 \theta_{\alpha} \sigma^{r,\alpha} \quad (26)$$

$$\sigma_{II} = \sum_{\alpha} \zeta_{\alpha} \sin^2 \theta_{\alpha} \sigma^{r,\alpha} \quad (27)$$

Since $\zeta_{\alpha} \geq 0$ and $\sum_{\alpha} \zeta_{\alpha} = 1$, we have:

$$\begin{aligned} \sigma_I + \sigma_{II} &= \sum_{\alpha} \zeta_{\alpha} \sigma^{r,\alpha} \\ &\leq f_t \sum_{\alpha} \zeta_{\alpha} = f_t \\ -\sigma_I - \sigma_{II} &= \sum_{\alpha} \zeta_{\alpha} (-\sigma^{r,\alpha}) \\ &\leq f_c \sum_{\alpha} \zeta_{\alpha} = f_c \\ \sigma_I/f_t - \sigma_{II}/f_c &= \sum_{\alpha} \zeta_{\alpha} (\cos^2 \theta_{\alpha} \sigma^{r,\alpha}/f_t - \sin^2 \theta_{\alpha} \sigma^{r,\alpha}/f_c) \\ &\leq \sum_{\alpha} \zeta_{\alpha} = 1 \\ \sigma_I/f_t - \sigma_{II}/f_c &= \sum_{\alpha} \zeta_{\alpha} (-\cos^2 \theta_{\alpha} \sigma^{r,\alpha}/f_c + \sin^2 \theta_{\alpha} \sigma^{r,\alpha}/f_t) \\ &\leq \sum_{\alpha} \zeta_{\alpha} = 1 \end{aligned}$$

So that $\boldsymbol{\sigma} \in G^{L_1\text{-Rankine}}$. \square

Finally, let us note that in the case where the consider family of reinforcement is discrete $\alpha \in \{\alpha_1, \dots, \alpha_N\}$, we only have that $\text{conv}_{\alpha} \{G^{\alpha}\} \subseteq G^{L_1\text{-Rankine}}$